JGR Solid Earth

RESEARCH ARTICLE
10.1029/2019JB017576

Special Section:
Physical Properties of Rocks, Friction and Fracturing: the Walsh Volume

H-D Interdiffusion in Single-Crystal Olivine: Implications for Electrical Conductivity in the Upper Mantle

Wei Sun[1,2], Takashi Yoshino[2], Minami Kuroda[3], Naoya Sakamoto[4], and Hisayoshi Yurimoto[3,4]

[1]Geodynamics Research Center, Matsuyama, Japan, [2]Institute for Study of the Earth's Interior, Okayama University, Tottori, Japan, [3]Department of Natural History Sciences, Hokkaido University, Sapporo, Japan, [4]Isotope Imaging Laboratory, Creative Research Institution, Hokkaido University, Sapporo, Japan

Key Points:
- The H diffusivity in olivine has an activation energy smaller than the previous work and demonstrates a positive correlation with water content
- The H diffusivity indicates a change of dominant diffusion mechanism at >1,000 K
- The H diffusivity cannot explain alone the observed extreme conductive anomalies in the asthenosphere

Supporting Information:
- Supporting Information S1
- Data Set S1

Correspondence to:
W. Sun,
diosgrc@hotmail.com

Citation:
Sun, W., Yoshino, T., Kuroda, M., Sakamoto, N., & Yurimoto, H. (2019). H-D interdiffusion in single-crystal olivine: Implications for electrical conductivity in the upper mantle. *Journal of Geophysical Research: Solid Earth*, *124*, 5696–5707. https://doi.org/10.1029/2019JB017576

Received 20 FEB 2019
Accepted 24 MAY 2019
Accepted article online 4 JUN 2019
Published online 29 JUN 2019

Abstract Knowledge of water content and distribution in the Earth's mantle is critical to understanding the geochemical evolution and geodynamic processes of the Earth, since water can incorporate into nominally anhydrous minerals at high pressure and dramatically affect the chemical and physical properties of mantle minerals. Hydrogen diffusion controls the transport of water and electrical conductivity in the deep Earth but is not fully understood for olivine, the most abundant mineral in the upper mantle. Here we present new hydrogen self-diffusion coefficients determined from interdiffusion in H- and D-doped olivine single-crystal couples at the upper mantle conditions (3–13 GPa and 1,000–1,300 K). Present activation enthalpy for hydrogen migration is significant smaller than previous work determined within a limited measured temperature range. Parallel interdiffusion experiments with diversified water concentrations demonstrated that hydrogen diffusivity strongly accelerated by the water content in olivine. The geometric average diffusion coefficient on olivine is showed as a function of temperature and water content: $D_{\mathrm{H}} = 10^{-7.4\pm0.8} * (C_{\mathrm{H_2O}})^{0.41\pm0.01} \exp\left(-\frac{130\pm17\ \mathrm{kJ/mol}}{\mathrm{RT}}\right)\ \mathrm{m^2/s}$. Combined with the Nernst-Einstein relation, the present results can constrain the contribution of water to the electrical conductivity on olivine. It suggests that in situ conductivity measurements on hydrous olivine at low temperatures (<1,000 K) produced too low activation enthalpy to extrapolate to the higher temperatures. Comparison with previous results by conductivity measurements on single-crystal olivine suggests that the literature data except for Dai and Karato (2014) might overestimate water effect on conductivity because of heterogeneity of synthetic single crystals. Because of a change of dominant hydrogen diffusion mechanism at high temperature, this study suggests that the modeling of mantle conductivity with a high activation enthalpy from diffusion data is more trustworthy. Considering a reevaluated activation enthalpy on hydrogen diffusion and water solubility in olivine, comparisons between present conductivity model and geophysical observations suggest that hydration of olivine cannot account for extremely high conductive values (10^{-2}–10^{-1} S/m) observed in the oceanic asthenosphere.

1. Introduction

Positive correlation between pressure and hydrogen solubility in nominally anhydrous minerals (e.g., Hirschmann et al., 2005) suggests a possibility that water can be stored at the deep Earth, which is supported by minerals found in mantle xenoliths, including olivine, which are brought to surface by alkaline or kimberlitic magma eruptions, which contain up to hundreds of ppm wt water (Bell & Rossman, 1992). Since incorporated water, even with those low concentrations, could largely affect elastic properties, electrical conductivity, melting behavior, and so on (Keppler & Smyth, 2006), knowledge of water content and distribution in the mantle is essential to understand the global geodynamics in the deep Earth.

Among many physical properties, proton conductivity, which is profited from hydrogen self-diffusivity and accelerated by water content (Karato, 1990), has been paid more attentions during the last decades because it is sensitive to the water content. Therefore, electrical conductivity becomes a powerful tool to constrain water content in the mantle, by comparison between magnetotelluric observations and laboratorial determinations on mantle minerals. On the account of elevated water solubility with pressure, proton conductivity is likely to be the most effective mechanism on bulk conductivity at the mantle condition (Gardés et al., 2014). Thus, the high electrical conductivities observed in the upper mantle (Evans et al., 2005; Ichiki et al., 2006; Naif et al., 2013; Tarits et al., 2004) has been explained by the incorporation of trace

amounts of hydrogen in olivine, the dominant upper mantle phase by some laboratorial determinations (Dai & Karato, 2014a, 2014b, 2014c; Wang et al., 2006). In contrast, this hypothesis was argued against by other studies, which reported much weaker water effect on electrical conductivity and concluded that hydration of olivine by itself was insufficiently to explain conductive anomalies in the upper mantle (Poe et al., 2010; Yoshino et al., 2006, 2009). The follow-on work from Gardés et al. (2014) attributed the debate to the uncertainty of water content determination and obtained an intermediate water effect on olivine conductivity through averaging the summarized literature data. However, without considering the rationality of experimental procedures of the literatures, the conclusion from Gardés et al. (2014) is not so convictive. Actually, the debate on water effect is difficult to be resolved from only in situ electrical conductivity measurements because dehydration unavoidably occurs during heating. Especially for high-temperature measurements on fine-grained polycrystal samples (Dai & Karato, 2014b, 2014c; Wang et al., 2006), the measured values were easily disturbed by grain boundary mechanism (Sun et al., 2018; Yoshino & Katsura, 2013).

Based on Nernst-Einstein relation, hydrogen self-diffusion in olivine provides an alternative method for determining electrical conductivity that circumvents the above experimental difficulties associated with previous in situ electrical conductivity measurements (Du Frane & Tyburczy, 2012; Novella et al., 2017). Hydrogen self-diffusivity is obtained from H-D interdiffusion experiments by employing diffusion couples composed of H- and D-doped single crystals that include negligible contribution of grain-boundary diffusion (Sun et al., 2015, 2018). Although diffusion data for olivine are available in a recent literature (Novella et al., 2017), previous study has been limited to a very narrow temperature range (150 K) and hence was difficult to provide well constrain on activation energy for hydrogen diffusion, which is critical to derive mineralogical models at the temperature of the upper mantle. Moreover, the previous work conducted actual H-D exchange experiments rather than H-D interdiffusion ones because only H-doped single-crystal olivine was used for one semi-infinite end, whereas another semi-infinite end was controlled by deuteroxide bath. In this case, the composition of semi-infinite end, C_1 buffed by deuteroxide bath, can only be coarsely estimated from diffusion profile trend in previous work rather than direct determination by secondary ion mass spectrometry (SIMS) as this study. C_1 is essential for fitting of hydrogen diffusion profile based on Fick's second law (Crank, 1975) so that indeterminism of C_1 largely constrained the validity for approximating hydrogen self-diffusion in previous work (Novella et al., 2017). In order to eliminate the above disadvantage from previous works, we employed both H- and D-doped single crystals for two semi-infinite ends in H-D interdiffusion experiments, which realized a determination of C_1 by SIMS. On the other hand, the temperature range investigated by this study was expanded twice than the previous work (Novella et al., 2017), which is important to determine reliable activation enthalpy for hydrogen diffusion. Moreover, the parallel experiments with diversified water contents have been performed in order to elucidate effect of water content on hydrogen self-diffusivity, which has been urgently required but poorly constrained by in situ conductivity measurements (Dai & Karato, 2014a; Gardés et al., 2014; Poe et al., 2010; Wang et al., 2006; Yoshino et al., 2009). All of the above contribute significantly to justifying the use of the Nernst-Einstein relation for electrical conductivity and hydrogen diffusion data to model mantle electrical conductivity and further help us to constrain water content in the upper mantle.

2. Experimental Approach

2.1. Synthesis of H- and D-Doped Olivine Single Crystals

For SIMS analysis, the olivine single crystal should be large and contain sufficient amount of water. Since H_2O solubility in olivine increases with increasing pressure (e.g., Hirschmann et al., 2005), we performed synthesis experiment of hydrous olivine single crystals in a wide pressure range from 3 to 13 GPa. At first, a traditional method that anneals dry single crystals in wet condition was used (Du Frane & Tyburczy, 2012; Novella et al., 2017). However, the recovered crystals at high pressures (>8 GPa) were rich in cracks and transferred to hydrous polycrystals. We modified to the thermal gradient method (Shatskiy et al., 2009), which was employed by pervious diffusion researches on wadsleyite and ringwoodite (Sun et al., 2015, 2018). Starting material consisted of silicate source plus water source, which composed of San Carlos olivine powder and oxide mixtures of brucite, quartz, and ferrous oxide, respectively. The bulk water content in the starting material was 2–3 wt.%. To prevent iron loss, the mixture was surrounded by Re foil (0.2-mm thickness) and loaded into a Pt capsule. The welded Pt capsule (3 mm in length and diameter)

Table 1
Water Content of Synthetic H-Doped and D-Doped Olivine Single Crystals Determined by Fourier-Transformed Infrared, and the Results of H-D Interdiffusion Runs Conducted in a Kawai-Type Multianvil Apparatus.

Synthesis					
Run		*P* (GPa)	*D*/(H + D)		Bulk (ppmw)
1k2368	H-ol	3	n.d.		150 ± 13
1k2370	D-ol	3	0.76 ± 0.03		136 ± 17
1K2442	H-ol	8	n.d.		557 ± 28
1K2450	D-ol	8	0.76 ± 0.02		519 ± 44
1K1841	H-ol	13	n.d.		1614 ± 127
1K1843	D-ol	13	0.74 ± 0.02		1648 ± 110
H-D Interdiffusion					
Run	***P* (GPa)**	**Axis**	***T* (K)**	***t* (min)**	**logD (m^2/s)**
1k2402	3	*a*	1,000	15	−12.54 ± 0.02
5k2697	3	*c*	1,000	25	−13.52 ± 0.04
1k2470	8	*a*	1,000	52	−12.34 ± 0.02
1k2473	8	*a*	1,100	25	−11.55 ± 0.01
1k2472	8	*a*	1,300	5.5	−10.63 ± 0.01
1k2466	8	*b*	1,000	65	−12.97 ± 0.03
1k2467	8	*b*	1,100	31	−12.48 ± 0.02
1k2471	8	*b*	1,300	7	−11.16 ± 0.02
1k2453	8	*c*	1,000	90	−13.19 ± 0.02
1k2454	8	*c*	1,200	12	−12.19 ± 0.02
1k2465	8	*c*	1,300	10	−12.11 ± 0.02
1k2129	13	*a*	1,000	80	−12.24 ± 0.02
5k2504	13	*c*	1,000	68	−12.93 ± 0.02

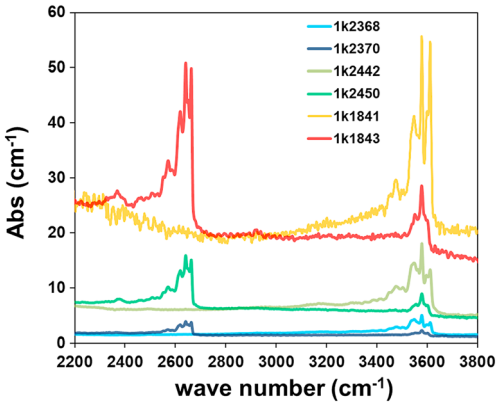

Figure 1. Unpolarized Fourier-transformed infrared spectra of H- and D-doped olivine single crystals with different water contents. Abs is the absorption coefficients, which are normalized to the sample thickness of 1 cm.

was loaded in an MgO sleeve surrounded by a stepped $LaCrO_3$ cylindrical heater. Crystal growing at high temperature profited from a monotonic thermal gradient, which was created by shifting the center of the capsule ~0.6 mm from the center of the heater along the axial direction. The silicate and water sources were placed in the hotter and colder regions in Pt capsule, respectively, so that recrystallization occurred at the colder region at the target temperature. The key point of this design was employing stepped $LaCrO_3$ heater, which accounted for a gentle thermal gradient and largely raised the possibility of gradual crystal growing rather than nucleation. A Cr-doped MgO octahedron with edge lengths of 18 mm and tungsten carbide cubes with truncation edge lengths of 11 mm were employed to generate 3, 8, and 13 GPa in a Kawai-type multianvil apparatus. Temperature was set to be 1,623 K with a holding duration of >8 hr. Most of synthetic olivine single crystals are transparent and free from inclusions, of which the largest grain size is ~1 mm. The homogeneity of olivine single crystals was confirmed by unpolarized Fourier-transformed infrared spectroscopy (Table 1 and Figure 1), and water contents were calculated based on a Paterson's calibration (Paterson, 1982).

2.2. H-D Interdiffusion Experiment

In order to investigate the anisotropy of hydrogen self-diffusion, the crystallographic orientations of olivine single crystals were determined using a precession camera. The orientated H- and D-doped crystals were double-polished along the same orientation with 1-μm diamond paste and put into a gold capsule. The crystals were tightly coupled together through gently compressing the fine-grained gold powder (1 μm) surrounding the crystal couples. Although straight $LaCrO_3$ heaters were used for diffusion experiments, the influence of thermal gradient was not expected to be crucial because of short length of the crystal couples (<0.8 mm). In interdiffusion experiments, we employed the same edge length of the octahedral and the cube truncation as synthesis to generate the pressure at 3, 8, and 13 GPa in a Kawai-type multianvil apparatus. Thermal properties of H-D interdiffusion were investigated by varying annealing temperature from 1,000 to 1,300 K. The heating rate was set to be >10 K/s in order to minimize diffusion during heating up to the target temperature, and the quenching was realized by cutting power off after annealing.

Recovered samples were polished to the center of diffusion couples. In order to minimize hydrogen background during SIMS analysis, the polished couples were mounted in Bi-Sn alloy with coating Au layers of ~30 nm by plasma sputtering. The SIMS of Cameca 6f and 1270 at Hokkaido University was employed to determine the H-D interdiffusion profiles. A primary Cs^+ ion beam operated at 17–20 nA was focused to form an array of spot analyses (20–30-μm spot size) on the sample along from one crystal edge to another perpendicular to the interface (Figure 2). The charge compensation was realized by a normal incident electron flood gun. In order to minimize artifacts arising from adsorbed hydrogen on the polished sample surface, a mechanical aperture was employed during collecting secondary ^1H, ^2H, and ^{30}Si ions from the center region (10 μm in diameter) of the sputtered area. The entrance and exit slits were set to be narrow enough to minimize the contribution of $^{28}Si^2H$ to the ^{30}Si. We did not use standard for line analysis because absolute concentrations are not essential for determinations of H-D interdiffusivity. Because of limited water solubility of olivine at low pressure, qualitative ^1H profiles failed to be determined for experiments at 3 GPa. Since bulk water content in D-doped and H-doped single crystals are similar (Table 1), diffusion profiles for experiments at 3 GPa were obtained from ratio of $^2H/^{30}Si$, which were same as Du Frane and Tyburczy (2012) and

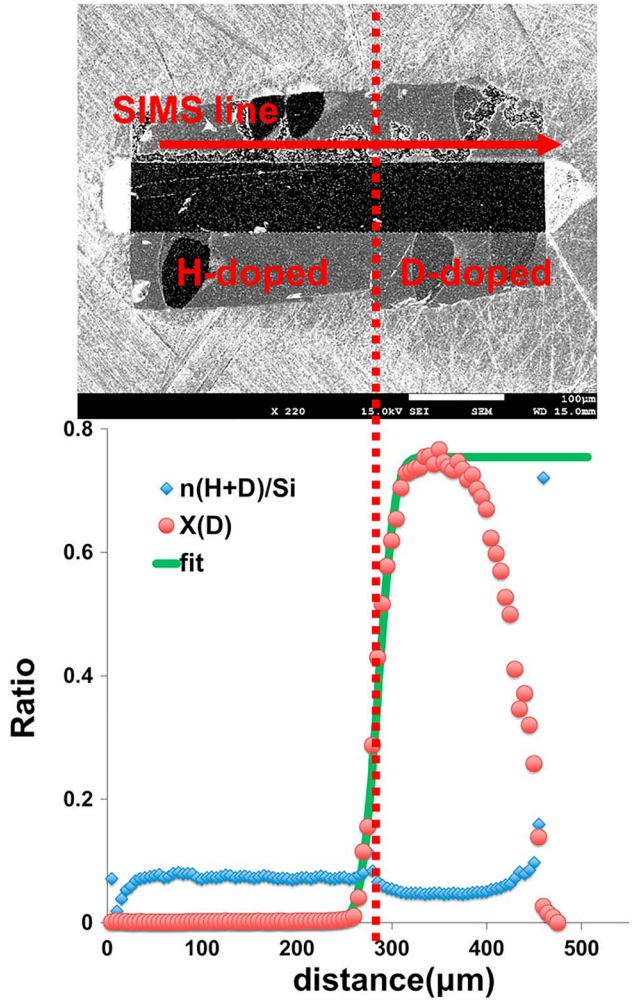

Figure 2. An example of interdiffusion profile in olivine from Run#1K2467 measured by SIMS. The upper image shows the secondary electron image of the sample, and the lower one shows the corresponding H-D interdiffusion profile. Horizontal darker area in the center part of sample corresponds to the damaged area analyzed by SIMS to obtain the interdiffusion profile. The other darker spots indicate the damaged area analyzed by SIMS to try obtaining the absolute H and D concentrations. Red circles are the normalized deuterium fraction X(D) at distance x (μm), and blue diamonds are count ratios between bulk hydrogen and ^{30}Si, which represent bulk water (H + D) distribution. X(D) in the center of the D-doped single crystal (flat region in red profile) is similar with the initial deuterium faction, ~0.76, suggesting that semi-infinite condition was well maintained during H-D interdiffusion. A similar profile at the opposite side of the interface represent an unavoidable exchange between D-doped crystal and residual water in gold powder with natural isotopic composition.

Novella et al. (2017), while diffusion profiles for experiments at 8 and 13 GPa were determined directly from ratio of ^{2}H/(^{1}H + ^{2}H).

3. Results

3.1. Hydrogen Self-Diffusion Coefficient in Olivine

H-D interdiffusion coefficients were determined by fitting interdiffusion profiles based on Fick's second law for a semi-infinite material (Crank, 1975). Concentration along x direction perpendicular to the interface is

$$\frac{C_{(x,t)}-C_0}{C_1-C_0}=\frac{1}{2}\,\mathrm{erfc}\left(\frac{x}{2\sqrt{D_{\mathrm{H-D}}t}}\right), \tag{1}$$

where $C_{(x,t)}$ is the normalized deuterium fraction ($\frac{C_D}{C_H+C_D}$) at distance x (m) and time t (s), C_0 is the initial deuterium fraction in H-doped crystal (set to 0), C_1 is the initial deuterium fraction in D-doped crystal (set to 1), and D_{H-D} is H-D interdiffusion coefficient. Figure 2 shows an example of an interdiffusion profile across H- and D-doped olivine single crystals. Because H-D interdiffusion coefficient is ~0.1 log units faster than hydrogen self-diffusion coefficient (Du Frane & Tyburczy, 2012),

$$\log D_{\mathrm{H}} = \log D_{\mathrm{H-D}} + 0.08, \tag{2}$$

where D_H is hydrogen self-diffusion coefficient. We obtained hydrogen self-diffusion coefficients at 8 GPa from 1,000 to 1,300 K (Figure 3) to the Arrhenius equation (3) and determine the preexponential term D_0 and activation enthalpy H_a for each crystallographic orientation:

$$\log D_{\mathrm{H}(T)} = \log D_0 - \frac{H_a}{2.303{*}RT}. \tag{3}$$

There is ~1 order of magnitude anisotropy on hydrogen self-diffusivities along each crystallographic orientation, at temperatures relevant to the upper mantle (Figure 3). The fastest hydrogen mobility demonstrated to be along [100] orientation, whereas the slowest hydrogen mobility was along the [001] orientation.

$$D_{\mathrm{H[100]}} = 10^{-5.0\pm0.5}{*}\exp\left(-\frac{140\pm11\mathrm{kJ/mol}}{\mathrm{RT}}\right)\mathrm{m^2/s}, \tag{4}$$

$$D_{\mathrm{H[010]}} = 10^{-5.1\pm1.0}{*}\exp\left(-\frac{153\pm21\mathrm{kJ/mol}}{\mathrm{RT}}\right)\mathrm{m^2/s}, \tag{5}$$

$$D_{\mathrm{H[001]}} = 10^{-8.2\pm0.9}{*}\exp\left(-\frac{95\pm19\mathrm{kJ/mol}}{\mathrm{RT}}\right)\mathrm{m^2/s}. \tag{6}$$

Hydrogen self-diffusivities of the three principal crystal orientations at 8 GPa are comparable with the previous ones at 2 GPa (Du Frane & Tyburczy, 2012) and 3 GPa (Novella et al., 2017; Figure 3). However, the obtained activation enthalpies of hydrogen self-diffusion are significantly smaller than the previous determinations (229 ± 18, 172 ± 19, and 188 ± 8 kJ/mol for [100], [010], and [001], respectively) from a narrow temperature range (Novella et al., 2017). The discrepancy between this study and Novella et al. (2017) could be attributed to the difference of measured temperature range and water content of olivine. Single crystals employed in this study have significantly higher water content than the ones from Novella et al. (2017; 74 ppmw). The activation enthalpy determined by this study might be smaller because of a lowering of activation energy of proton migration as water content increases (more details seen in section 4.2; Poe et al., 2010; Yoshino et al.,

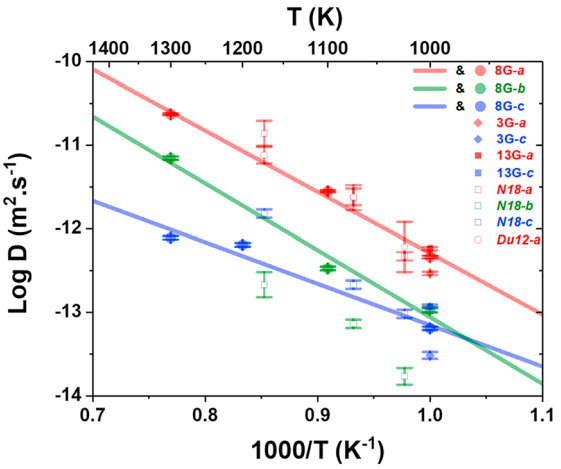

Figure 3. Arrhenius plots of hydrogen self-diffusion for three principal crystallographic orientations of olivine. Colors red, green, and blue represent [100], [010], and [001] orientations, respectively. The solid diamonds, solid circles, and solid squares represent hydrogen self-diffusion coefficients from this study at 3, 8, and 13 GPa, respectively. The hollow diamonds and squares are hydrogen self-diffusion coefficients referred from Du Frane and Tyburczy (2012) and Novella et al. (2017), respectively.

2009). Since diffusion for water incorporation mechanism can have higher activation energy than hydrogen self-diffusion, the other possible reason is that *Novella's* diffusion profile possibly included the concentration diffusion. The anisotropy between [010] and [001] orientations observed in this study is a contrast to the result from Novella et al. (2017; Figure 3), which cannot be explained by difference of the measured temperature range for each study. We noticed that our data for [010] agreed well with the ones for [001] from Novella et al. (2017; especially for data at 3 GPa), while our data for [001] agreed with their data for [010]. Two models were introduced to calculate the average of the three principal crystal orientations:

$$D_{\mathrm{Hp}} = \frac{D_{\mathrm{H[100]}} + D_{\mathrm{H[010]}} + D_{\mathrm{H[001]}}}{3}, \tag{7}$$

$$D_{\mathrm{Hg}} = \sqrt[3]{D_{\mathrm{H[100]}} D_{\mathrm{H[010]}} D_{\mathrm{H[001]}}}, \tag{8}$$

where D_{Hp} is arithmetic average self-hydrogen diffusivities and D_{Hg} is the geometric average self-hydrogen diffusivities. Linear Arrhenius fitting yields the preexponential term, $D_{0\mathrm{p}} = 10^{-5.4 \pm 0.5}$ m^2/s, the activation enthalpy, $H_{ap} = 140 \pm 11$ kJ/mol (defined temperature is from 1,000 to 1,300 K) and $D_{0\mathrm{g}} = 10^{-6.1 \pm 0.8}$ m^2/s, and the activation enthalpy, $H_{ag} = 130 \pm 17$ kJ/mol, respectively.

3.2. Water Content Dependence on Hydrogen Self-Diffusivity

Recent studies have advocated water content acceleration in proton diffusivity of olivine; this hypothesis is supported by our results. The water contents in synthetic olivine distinguish among different synthetic pressures (Table 1). At 1,000 K, hydrogen self-diffusivities increase as water content increases for both [100] and [001] orientations (Figure 4). Previous studies suggested that pressure dependence cannot account for this acceleration because of tiny negative correlation between pressure and proton diffusivity, which is opposite with our observation (Dai & Karato, 2014b). Thus, this study demonstrated the increase of hydrogen self-diffusion coefficient to acceleration from water content. The water content dependence of hydrogen diffusivities could be attributed to a lowering of activation energy of proton migration as water content increasing, which has been reported in olivine by electrical conductivity measurements (Poe et al., 2010; Yoshino et al., 2009). Since such effect has been also observed in ringwoodite but not in wadsleyite (Yoshino et al., 2008), the water content dependence of hydrogen diffusivities of olivine might be attributed to a change of dominant hydrogen configuration in the crystal structure with increasing water content. NMR spectroscopy suggested that hydrogen should occupy Mg-site vacancies in wadsleyite (Sano-Furukawa et al., 2011), whereas they should occupy vacancies of mostly Si-site in olivine (Xue et al., 2017) and those of Mg- and Si-sites in ringwoodite (Purevjav et al., 2014). Because the hydrogen incorporation mechanism of olivine is still unknown, we cannot provide an appropriate formula to express the water content dependence of hydrogen diffusion at present. Based on the empirical Arrhenius equation (9),

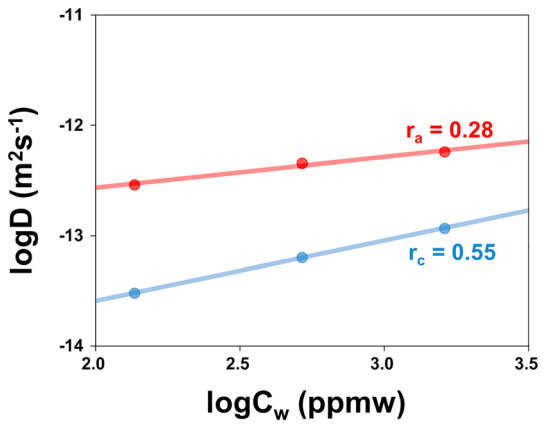

Figure 4. Hydrogen self-diffusivities of olivine at 1,000 K as a function of log water content in olivine crystal couples. Colors red and blue represent [100] and [001] orientations, respectively.

$$D_{\mathrm{H}(T)} = D_0 (C_H)^r \exp\left(-\frac{H_a}{\mathrm{RT}}\right), \tag{9}$$

where C_H is the water content of olivine in unit of ppm wt and r is the water content exponent. The fitted water content exponent r equals to 0.28 ± 0.03 and 0.55 ± 0.01 for [100] and [001] orientations, respectively (Figure 4). This result suggests that the anisotropy of hydrogen self-diffusion decreases with increasing water content. The isotropic water content exponent r_g is calculated on average of [100] and [001] orientations, equals to 0.41 ± 0.01, which is employed in the geometric mean model.

Sample water content from the use of the IR calibration of Paterson (1982) on olivine has been proposed to underestimate by a factor of 2–4 (Bell et al., 2003). Based on water partition coefficient between olivine and pyroxene, a factor 3 was frequently employed in previous works (Ardia et al., 2012; Férot & Bolfan-Casanovaet, 2012; Hirschmann et al., 2005). Thus, water contents in olivine multiply by a factor of 3 and the geometric average diffusion coefficient D_{Hg} is shown as a function of temperature and water content:

$$D_{\mathrm{Hg}} = 10^{-7.4\pm0.8} * (C_H)^{0.41\pm0.01} \exp\left(-\frac{130\pm17\mathrm{kJ/mol}}{\mathrm{RT}}\right) \mathrm{m}^2/\mathrm{s}, \quad (10)$$

4. Discussion

4.1. Implications for Electrical Conductivity in Olivine

Theoretically, proton conductivity and hydrogen self-diffusivity in nominally anhydrous minerals can be expressed by the Nernst-Einstein equation (Karato, 1990).

$$\sigma_{\mathrm{H}} = \frac{D_{\mathrm{H}} C_{\mathrm{H}} q^2}{kT}, \quad (11)$$

where σ_{H} is the proton conductivity, D_{H} is the hydrogen self-diffusion coefficient, C_{H} is the concentration of hydrogen, q is charge, k is the Boltzmann constant, and T is absolute temperature. The electrical conductivity of mantle olivine as a function of temperature is estimated by combining the conductivity of dry olivine with the proton conductivity:

$$\sigma = \sigma_{\mathrm{H}} + \sigma_{\mathrm{dry}}, \quad (12)$$

where σ is the total conductivity of hydrated olivine and σ_{dry} is the conductivity of dry olivine. In this study, electrical conductivity of dry olivine was referred from Yoshino et al. (2009). Arithmetical and harmonic mean conductivity σ_{p} and σ_{g} were estimated from D_{Hp} and D_{Hg}, respectively. Water content exponent r obtained from [100] orientation was employed in σ_{p} because arithmetical geometric mean is dominated by the fastest [100] orientation. Correspondingly, isotropic water content exponent r_g was employed in σ_{g}. Since sample water content from the use of the IR calibration of Paterson (1982) on olivine has been proposed to underestimate by a factor of 2–4 (Bell et al., 2003), a factor 3 was applied to estimate water contents in diffusion couples for water correction. This factor is not sensitive to the conclusions from comparison with previous works, which is shown in Figure 5d. Since unavoidable dehydration occurred at the high temperature, electrical conductivity measured at >1,000 K on hydrous olivine polycrystals is easily contaminated by mobility of hydrogen trapped within grain boundary, which is >5 log unit faster than lattice self-diffusion (Demouchy, 2010). Dai and Karato (2014a) reported that electrical conductivity on single crystals of hydrous olivine is ~1 order unit lower than their results on polycrystals by the same authors (Dai & Karato, 2014b, 2014c). The most likely explanation is that there was contribution from grain boundary hydrogen in fine-grained polycrystal measurements. Therefore, these high-temperature works especially with fine grain size (<5 μm; Dai & Karato, 2014b, 2014c; Wang et al., 2006) were not summarized for comparison.

As shown in Figure 5, although electrical conductivities of hydrous olivine estimated from hydrogen self-diffusivities are comparable between this study and Novella et al. (2017) at the measured temperature range, our result yields significantly lower values than the estimation from Novella et al. (2017) once extrapolating to the upper mantle geotherm because activation enthalpy determined by this study is considerably smaller. At 1,000 K, the electrical conductivities of hydrous olivine estimated from hydrogen self-diffusivities agree well with the data of Yoshino et al. (2009) and Dai and Karato (2014a) at a wide range of water content (Figure 5). Although our result is consistent with the data of Poe et al. (2010) at a low water content, the difference between these two works raised markedly as water content increases because previous works reported stronger accelerated effect from water content. There is large debate (~1.5 log units) between our result and the data from Yang (2012) at a wide range of water content. This discrepancy is difficult to be explained by uncertainty of water content estimation from various calibrations. Since Yang (2012) employed single crystals and performed conductivity measurements at <1,000 K, influence from grain boundary mechanism is thought to be large and the origin of discrepancy needs a further exploration.

To obtain large hydrous single crystals, a common method is annealing dry single crystal under water-saturated condition (Dai & Karato, 2014a; Du Frane & Tyburczy, 2012; Novella et al., 2017; Poe et al.,

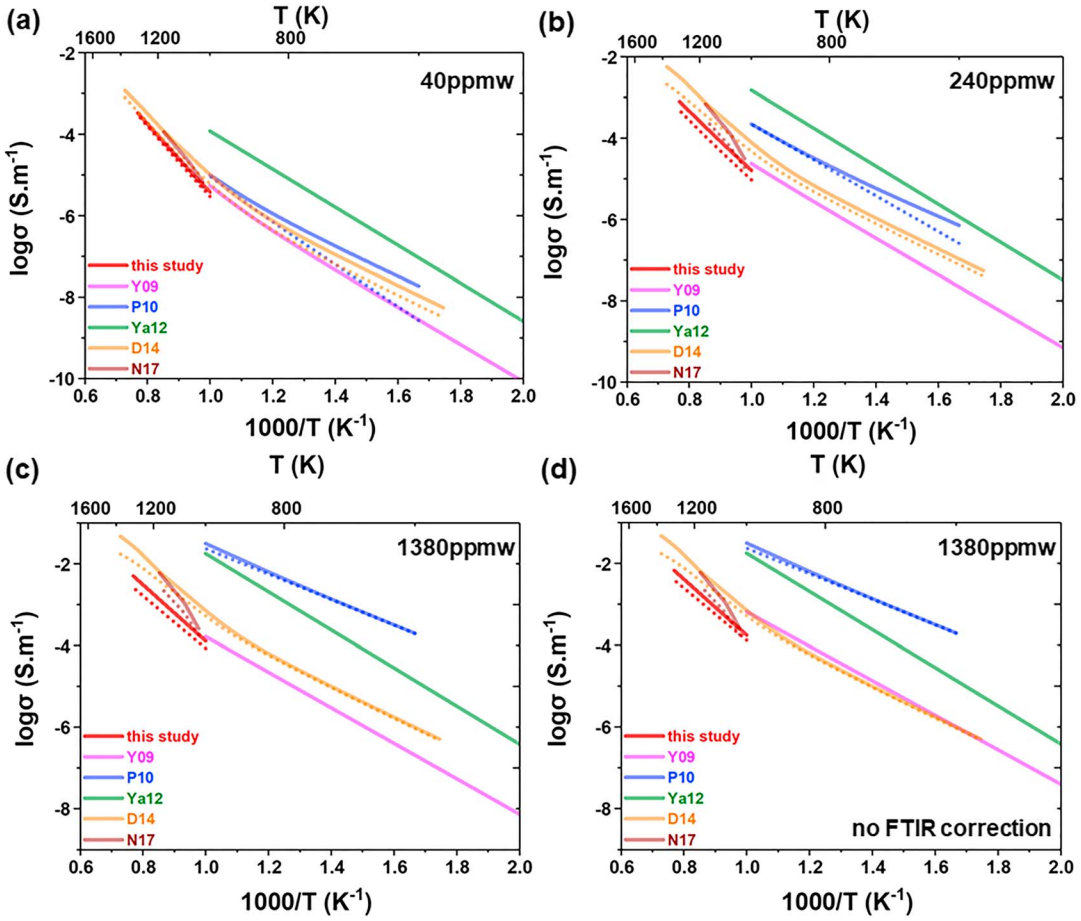

Figure 5. Electrical conductivity of olivine as functions of temperature with different water contents (a) 40 ppm wt, (b) 240 ppm wt, (c) 1,380 ppm wt, and (d) 1,380 ppm wt (without water content correction on unpolarized Fourier-transformed infrared determinations) in a comparison with previous studies. Y09, P10, Ya12, D14, and N17 are referred from Yoshino et al. (2009), Poe et al. (2010), Yang (2012), Dai and Karato (2014a), and Novella et al. (2017), respectively. Solid and dotted lines represent the arithmetic and geometic average conductivities, respectively. Dai and Karato (2014a) employed olivine single crystals with water content of 2,662, 1,678, and 3,761 ppm wt for conductivity measurements of [100], [010], and [001], respectively. The measurements were normalized to the values with a water content of 1,380 ppm wt, without considering water content acceleration effect ($r = 0$). In this study, we used the original data from Dai and Karato (2014a) for water correction, with water content exponents $r = 0.28$ and 0.55 for arithmetic average and geometric average, respectively. Since Yang (2012) reported isotopic conductivities on hydrous olivine, only geometric model is employed in average conductivities, as showed by green solid lines.

2010; Yang, 2012; Yoshino et al., 2006). In the previous interdiffusion experiments, additional dry annealing step at a very high temperature is employed to produce abundant Mg vacancies at first (Du Frane & Tyburczy, 2012; Novella et al., 2017) so that during wet annealing, surrounding hydrogen can incorporate into single crystals through a fast redox mechanism (Kohlstdt & Mackwell, 1998). Otherwise, hydration process is dominated by a much slower vacancy mechanism (Demouchy & Mackwell, 2003, 2006). Since synthesis of single crystal in previous studies did not contain a dry annealing step and the homogeneity of synthetic hydrous single crystals for conductivity measurements are profoundly questioned. The appropriate solution to investigate homogeneity of the sphere is given by Crank (1975) as following equation:

$$C_{(t)} = 1 + 2\sum_{1}^{n}(-1)^n \exp\left(-\frac{D_H^{eff} n^2 \pi^2}{d^2}\right), \tag{13}$$

where $C_{(t)}$ is normalized concentration, d is the radius of the sphere, and D_H^{eff} is effective hydrogen diffusivity. The equilibration time $t_{0.8}$ is defined as the time needed to equilibrate the grain to such an extent that the normalized concentration at the center is 0.8, which is thought to be a homogeneity condition. Since sample shape for conductivity measurement is cylinder that requires longer duration for equilibration instead of sphere, $t_{0.8}$ estimated from equation (13) is considered to be the lower limit for homogeneity. Figure 6

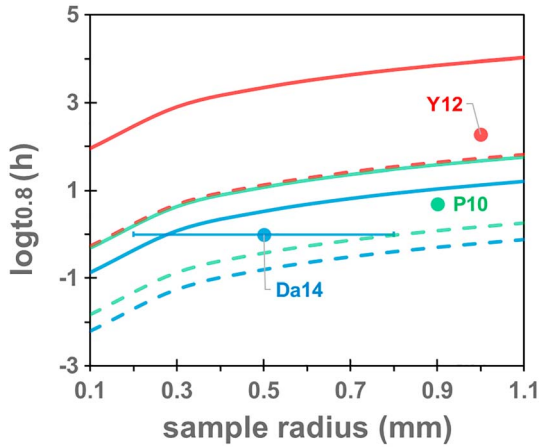

Figure 6. Equilibration time $t_{0.8}$ as a function of sample radius. Colors red, green, and blue points represent experimental conditions (sample sizes and annealing duration) referred from Yang (2012), Poe et al. (2010), and Dai and Karato (2014a), respectively. Since crystals used in pervious works were cylinder shape, the sample radiuses were chosen from half of the minimum between cylinder diameter and height. In this case, $t_{0.8}$ based on equation (13) could be thought to be the lower limit duration for homogeneity of samples. Dai and Karato (2014a) only reported sample sizes (1.6 mm in diameter and 0.4 mm in height) for electrical conductivity measurements instead of the one used in wet annealing. We used 0.5 ± 0.3 mm as the sample radius for Dai and Karato (2014a). Solid and dashed lines represent equilibration time for wet annealing without and with a predry-annealing step, respectively. Colors of lines suggest the simulations based on equation (13) employed hydrogen effective diffusion coefficients, corresponding to the annealing temperature reported in references.

shows a comparison between equilibration time $t_{0.8}$ and wet annealing duration in previous works. Without a dry annealing step, the durations of wet annealing adopted in Poe et al. (2010) and Yang (2012) were not enough, suggesting that samples measured in these studies were far from a homogeneity condition. Based on equation (13), the centers of olivine single crystals (~2-mm grain size) used in Poe et al. (2010) and Yang (2012) proved to be not hydrated at all and the homogeneity sizes was less than 0.6 and 0.3 mm after the annealing time adopted in these two works, respectively. It is not surprising that previous works overestimated conductivities on single crystals with sufficiently hydrated edge and poorly hydrated center.

Most of the conductivity measurements were performed at temperatures <1,000 K (Poe et al., 2010; Yang, 2012; Yoshino et al., 2006, 2009), and the obtained activation enthalpy is less than 100 kJ/mol, which is significantly lower than activation enthalpy (110–150 kJ/mol) from hydrogen diffusion experiments conducted at >1,000 K (Du Frane & Tyburczy, 2012; Novella et al., 2017). Karato (2013) advocated a hybrid hydrogen model to explain the enthalpy difference between hydrogen self-diffusion and electrical conduction. In olivine, besides Mg vacancy, hydrogen can also be activated to the interstitial site as free proton. Although the concentration of free proton is low, its extreme high mobility allows free proton mechanism to be effective in certain conditions. As temperature increases, the dominated diffusion mechanism could change from free proton mechanism to Mg vacancy mechanism or change from free proton mechanism to Mg vacancy mechanism. As a result, activation enthalpies change at the different temperature ranges. This hypothesis was supported by high-temperature conductivity measurements on single-crystal hydrous olivine (Dai & Karato, 2014a), which observed a mechanism transformation at ~1,000 K. At <1,000 K, most of the conductivity measurement yielded similar activation enthalpies to each other. At >1,000 K, the previous conductivity measurements displayed the similar anisotropy as this study, with the fastest orientation along [100] and the slowest along [001]. Both studies showed that the difference between [100] and [001] is ~1 log unit. The geometric average activation enthalpy determined from diffusivity (122 ± 17 kJ/mol) is also comparable with that from conductivity measurement (112 ± 5 kJ/mol) at the same temperature range (1,000–1,300 K; Figure 5c). Thus, consistency of the activation enthalpy between hydrogen self-diffusivity and electrical conductivity is likely to be on account of alteration of effective hydrogen diffusion mechanisms within different experimental temperatures.

On the other hand, the use of the Nernst-Einstein relation and hydrogen self-diffusivity to estimate electrical conductivity in mantle olivine has been also yielded a magnitude discrepancy, based on higher electrical conductivity results for hydrous olivine in comparison to estimations from hydrogen self-diffusivities (Gardés et al., 2014; Wang et al., 2006). In exchange among different elements, more atoms will be on one side of the interface after diffusion, which results in a net volume transport. Since nonuniform stress accumulates during exchange in responding to the concentration change, the bulk diffusion coefficient is constrained by the slowest element diffusivity and equals to a harmonic mean of diffusion coefficient of all elements. Karato (2013, 2015) introduced such mechanism into H-D interdiffusion and argued that the system strain energy was accumulating during H-D interdiffusion because the flux of hydrogen or deuterium species changes with position, causing a change in the concentration:

$$\sum \frac{\partial C_{iH}}{\partial t} = -\sum \frac{\partial}{\partial x} J_{iH} \neq 0 \tag{14}$$

$$\sum \frac{\partial C_{iD}}{\partial t} = -\sum \frac{\partial}{\partial x} J_{iD} \neq 0, \tag{15}$$

where $C_{iH(D)}$ is the concentration of the ith hydrogen (deuterium) species and $J_{iH(D)}$ is the flux of the ith hydrogen (deuterium). In this case, the bulk interdiffusion coefficient equals to a harmonic mean of

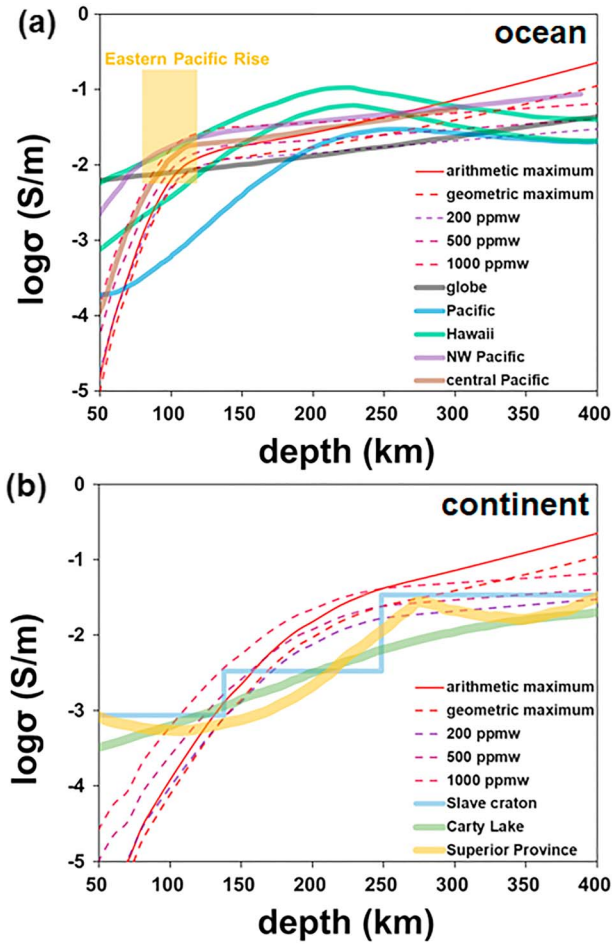

Figure 7. Comparison of electrical conductivity from hydrogen self-diffusivity of olivine as a function of water contents with the geophysically observed conductivity-depth profiles beneath the (a) ocean and (b) continent. Global model (Kuvshinov & Olsen, 2006), Hawaii (Lizarrlde et al., 1995), Pacific (Baba et al., 2010), NW Pacific (Baba et al., 2013), central Pacific (Sarafian et al., 2015), Eastern Pacific Rise (Evans et al., 2005), Slave craton (Jones et al., 2003), Carty Lake (Neal et al., 2000), and Superior Province (Schultz et al., 1993). Arithmetic and geometric maximum represent electrical conductivities of hydrous olivine with water content equal to solubility in olivine based on arithmetic and geometric mean models, respectively.

diversified hydrogen species. As a result, estimated conductivities from hydrogen diffusivities are lower than in situ measured ones, which equal to arithmetical means of different hydrogen species. However, this study argues against the above standpoint from both theory and practice. There is a significant difference between isotope interdiffusion and exchange among different elements. If the bulk isotopic concentrations at both sides are similar, the concentration changes of one isotope at a certain position during interdiffusion can be well compensated by another isotope. The resulting bulk strain accumulation on the account of volume change is significantly small, which has been confirmed by indistinguishable molecular volumes between H- and D-doped minerals (Sano-Furukawa et al., 2011):

$$\sum\left(\frac{\partial C_{iH}}{\partial t}+\frac{\partial C_{iD}}{\partial t}\right)=-\sum\frac{\partial}{\partial x}(J_{iH}+J_{iD})\approx 0. \tag{16}$$

Thus, there is no requirement to introduce a harmonic mean into a H-D interdiffusion. The bulk H-D interdiffusivity is also largely dominated by the fastest hydrogen diffusivity and represents an arithmetical average of all hydrogen species, which is same as electrical conductivity. Consequently, this consistency is expected between estimated conductivity from hydrogen self-diffusivity and the measured conductivity, which has been demonstrated in comparison between this study and pervious works (Dai & Karato, 2014a; Yoshino et al., 2009; Figure 5). The so-called debate on magnitude between estimations from hydrogen self-diffusivity and in situ conductivity measurements is no more than a disparate on in situ measured conductivities itself from various works (Figure 5), which is largely affected by heterogeneity of starting samples, incompatible measured temperatures, a variety of water content calibrations, and so on. From this study, the mean free terminal drift velocity of hydrogen isotopes would be the same in response to a chemical potential gradient or an electrical potential gradient, justifying the use of Nernst-Einstein relation to model electrical conductivity. Moreover, an increase of activation enthalpy in hydrous olivine at >1,000 K suggests that the exploration from conductivity measurements at <1,000 K is likely to underestimate the mantle conductivity. Alternatively, modeling mantle conductivity with a high activation enthalpy from diffusion data is more trustworthy.

4.2. Implications for Electrical Conductivity in the Upper Mantle

Since the temperature distributions are largely controlled by the conductive heat transfer in the lithosphere, the geotherm was determined from thermobarometry of mantle xenoliths for the continental mantle (Rudnick et al., 1998) and derived from surface heat flow for the oceanic mantle (Turcotte & Schubert, 1982). The geotherm in the deep regions was considered to be adiabatic, which was taken from Katsura et al. (2010). Although mantle oxygen fugacity is lower than that employed in H-D interdiffusion experiments of this study, oxygen fugacity dependence on hydrogen diffusion or proton conduction in olivine proved to be very weak especially at high temperatures (Dai & Karato, 2014c). We calculated hydrous olivine conductivity profiles along oceanic and continental geotherms based on hydrogen self-diffusivities without taking into account the oxygen fugacity effect. There is a positive correlation between depth and the concentration of water in olivine (the global model by Kuvshinov & Olsen, 2006). The estimated water content in the global model is less than 200 ppm wt at a shallow depth (<250 km). At regions deeper than 250 km it increases to ~500-ppm wt maximum at the boundary with the transition zone, which is consistent with the petrological models (Ardia et al., 2012; Hirschmann et al., 2009). Typical geophysical 1-D profiles for the upper mantle beneath the oceans (Baba et al., 2010; Kuvshinov & Olsen, 2006) and continents (Jones et al., 2003; Neal et al., 2000; Schultz et al., 1993) agree fairly well with the conductivities given by this study within this range (Figure 7). Most of the

geophysical data beneath the continents are compatible with olivine containing less than 500-ppm wt water in agreement with petrological predictions.

It is crucial to consider the geochemical and petrological constraints when interpreting geophysical conductivity data in terms of olivine hydration. We calculated the conductivity at the water storage capacity of olivine equilibrated in MgO–FeO–Al_2O_3–SiO_2–H_2O systems (Férot & Bolfan-Casanovaet, 2012) along oceanic and continental geotherms, which is the maximum conductivity of hydrous olivine before the exsolution of fluids or the onset of partial melting (Figure 7). High electrical conductivity anomalies were observed in the asthenosphere beneath continental lithosphere (Ichiki et al., 2006; Tarits et al., 2004) and beneath oceanic lithosphere (Evans et al., 2005; Naif et al., 2013), generally in the range of ~10–1.0 S/m. Based on a reevaluated activation enthalpy for hydrogen migration, our model suggests that the hydration of olivine by itself is not enough to explain these extreme conductive values in the asthenosphere. Our result is in contrast to recent work from Novella et al. (2017), who argued that 250-ppm wt water incorporated in olivine accounted for conductive anomalies in the asthenosphere based on an extrapolation along relative high activation enthalpy determined from a narrow temperature. Although our model took into account the water acceleration effect on hydrogen migration, the derived electrical conductivity with maximum water content was significantly lower than the geophysics observations (Figure 7a). The presence of a partial melt, induced by incorporation of water and aligned parallel to the plate motion, would be required to explain the high conductivity anomalies in the asthenosphere (Gaillard et al., 2008; Zhang et al., 2014). The conductivity-depth model beneath Hawaii (Lizarrlde et al., 1995), the northwestern and central Pacific (Baba et al., 2013; Sarafian et al., 2015) yielded higher conductivity values than our model accounted for the maximum water solubility of olivine in the upper mantle. Although Yoshino et al. (2008) argued that the presence of a hot plume beneath Hawaii (Fukao et al., 2001) could account for these conductive ranges between 150 and 250 km depth, the high-temperature region caused by plume is much more limited in comparison with the geophysical survey region. Therefore, thermal heterogeneity might not account for the high conductivity beneath Hawaii. Alternatively, either hydration-induced partial melt or carbonate melt might be more probable explanations for conductive regions observed beneath Pacific in the upper mantle (Gaillard et al., 2008; Zhang et al., 2014).

5. Conclusion

1. Significantly higher activation enthalpy for hydrogen diffusion was determined by analysis of H-D interdiffusion profiles conducted at a wider temperature in comparison with H-D exchange experiments by Novella et al. (2017). The water dependence on hydrogen self-diffusivity was identified from the parallel interdiffusion experiments with diversified water concentrations.
2. Combined with the Nernst-Einstein relation, the resultant conductivity suggests that the dominant mechanism of hydrogen migration changed at >1,000 K in comparison with in situ conductivity measurements. A change of hydrogen migration mechanism at high temperature could account for the debate between hydrogen diffusivity and electrical conductivity advocated by previous studies. The modeling of mantle conductivity from diffusion data with activation enthalpy higher than that from conductivity measured at low temperatures is more trustworthy.
3. According to a reevaluated activation enthalpy for hydrogen diffusion and limited water solubility in olivine in the upper mantle, comparisons between the present model and geophysical observations do not support hydration of olivine accounting for the conductivity profile observed in the asthenosphere and the conductive regions beneath the Pacific. Alternatively, additional mechanisms, for example, hydrous partial melt and carbonate melt, are required to explain the conductivity anomalies observed in the oceanic asthenosphere.

Acknowledgments
As per AGU's Data Policy, the data in this study are listed in the references and supporting information. The authors appreciate D. Yamazaki and N. Tsujino for beneficial discussions and S. Yamashita for measurements by Fourier-transform infrared spectroscopy. This work was supported by Grants-in-Aid for Scientific Research Grants JP15H05827 and 24244087 to T. Y. from the Japan Society for the Promotion of Science. We thank two anonymous reviewers who helped us improve the manuscript.

References

Ardia, P., Hirschmann, M. M., Withers, A. C., & Tenneri, T. J. (2012). H_2O storage capacity of olivine at 5–8 GPa and consequences for dehydration partial melting of the upper mantle. *Earth and Planetary Science Letters*, *345-348*, 104–116. https://doi.org/10.1016/j.epsl.2012.05.038

Baba, K., Tada, N., Zhang, L., Liang, P., Shimizu, H., & Utada, H. (2013). Is the electrical conductivity of the northwestern Pacific upper mantle normal? *Geochemistry, Geophysics, Geosystems*, *14*, 4969–4979. https://doi.org/10.1002/2013GC004997

Baba, K., Utada, H., Goto, T., Kasaya, T., Shimizu, H., & Tada, N. (2010). Electrical conductivity imaging of the Philippine Sea upper mantle using seafloor magnetotelluric data. *Physics of the Earth and Planetary Interiors*, *183*(1-2), 44–62. https://doi.org/10.1016/j.pepi.2010.09.010

Bell, D. R., & Rossman, G. R. (1992). Water in Earth's mantle: The role of nominally anhydrous minerals. *Science*, *255*(5050), 1391–1397. https://doi.org/10.1126/science.255.5050.1391

Bell, D. R., Rossman, G. R., Maldener, J., Endisch, D., & Rauch, F. (2003). Hydroxide in olivine: A quantitative determination of the absolute amount and calibration of the IR spectrum. *Journal of Geophysical Research*, *108*(B2), 2105. https://doi.org/10.1029/2001JB000679

Crank, J. (1975). *The Mathematics of Diffusion*. Oxford: Oxford University Press.

Dai, L., & Karato, S. (2014a). High and highly anisotropic electrical conductivity of the asthenosphere due to hydrogen diffusion in olivine. *Earth and Planetary Science Letters*, *408*, 79–86. https://doi.org/10.1016/j.epsl.2014.10.003

Dai, L., & Karato, S. (2014b). The effect of pressure on the electrical conductivity of olivine under the hydrogen-rich conditions. *Physics of the Earth and Planetary Interiors*, *232*, 51–56. https://doi.org/10.1016/j.pepi.2014.03.010

Dai, L., & Karato, S. (2014c). Influence of oxygen fugacity on the electrical conductivity of olivine: Implications for the mechanism of conduction. *Physics of the Earth and Planetary Interiors*, *232*, 57–60. https://doi.org/10.1016/j.pepi.2014.04.003

Demouchy, S. (2010). Diffusion of hydrogen in olivine grain boundaries and implications for the survival of water-rich zones in the Earth's mantle. *Earth and Planetary Science Letters*, *295*(1-2), 305–313. https://doi.org/10.1016/j.epsl.2010.04.019

Demouchy, S., & Mackwell, S. J. (2003). Water diffusion in synthetic iron-free forsterite. *Physics and Chemistry of Minerals*, *30*(8), 486–494. https://doi.org/10.1007/s00269-003-0342-2

Demouchy, S., & Mackwell, S. J. (2006). Mechanisms of hydrogen incorporation and diffusion in iron-bearing olivine. *Physics and Chemistry of Minerals*, *33*(5), 347–355. https://doi.org/10.1007/s00269-006-0081-2

Du Frane, W. L., & Tyburczy, J. A. (2012). Deuterium-hydrogen exchange in olivine: Implications for point defects and electrical conductivity. *Geochemistry, Geophysics, Geosystems*, *13*, Q03004. https://doi.org/10.1029/2011GC003895

Evans, R. L., Hirth, G., Baba, K., Forsyth, D., Chave, A., & Mackie, R. (2005). Geophysical evidence from the MELT area for compositional controls on oceanic plates. *Nature*, *437*(7056), 249–252. https://doi.org/10.1038/nature04014

Férot, A., & Bolfan-Casanovaet, N. (2012). Water storage capacity in olivine and pyroxene to 14 GPa: Implications for the water content of the Earth's upper mantle and nature of seismic discontinuities. *Earth and Planetary Science Letters*, *349-350*, 218–230. https://doi.org/10.1016/j.epsl.2012.06.022

Fukao, Y., Widiyantoro, S., & Obayashi, M. (2001). Stagnant slabs in the upper and lower mantle transition region. *Reviews of Geophysics*, *39*(3), 291–323. https://doi.org/10.1029/1999RG000068

Gaillard, F., Marki, M., Iacono-Marziano, G., Pichavant, M., & Scaillet, B. (2008). Carbonatite melts and electrical conductivity in the asthenosphere. *Science*, *322*(5906), 1363–1365. https://doi.org/10.1126/science.1164446

Gardés, E., Gaillard, F., & Tarits, P. (2014). Toward a unified hydrous olivine electrical conductivity law. *Geochemistry, Geophysics, Geosystems*, *15*, 4984–5000. https://doi.org/10.1002/2014GC005496

Hirschmann, M. M., Aubaud, C., & Withers, A. C. (2005). Storage capacity of H_2O in nominally anhydrous minerals in the upper mantle. *Earth and Planetary Science Letters*, *236*(1-2), 167–181. https://doi.org/10.1016/j.epsl.2005.04.022

Hirschmann, M. M., Tenner, T., Aubaud, C., & Withers, A. C. (2009). Dehydration melting of nominally anhydrous mantle: The primacy of partitioning. *Physics of the Earth and Planetary Interiors*, *176*(1-2), 54–68. https://doi.org/10.1016/j.pepi.2009.04.001

Ichiki, M., Baba, K., Obayashi, M., & Utada, H. (2006). Water content and geotherm in the upper mantle above the stagnant slab: Interpretation of electrical conductivity and seismic P-wave velocity models. *Physics of the Earth and Planetary Interiors*, *155*, 1–15. https://doi.org/10.1016/j.pepi.2005.09.010

Jones, A. G., Lezaeta, P., Ferguson, I. J., Chave, A. D., Evans, R. L., Garcia, X., & Spratt, J. (2003). The electrical structure of the Slave craton. *Lithos*, *71*(2-4), 505–527. https://doi.org/10.1016/j.lithos.2003.08.001

Karato, S. (1990). The role of hydrogen in the electrical conductivity of the upper mantle. *Nature*, *347*(6290), 272–273. https://doi.org/10.1038/347272a0

Karato, S. (2013). Theory of isotope diffusion in a material with multiple species and its implications for hydrogen-enhanced electrical conductivity in olivine. *Physics of the Earth and Planetary Interiors*, *219*, 49–54. https://doi.org/10.1016/j.pepi.2013.03.001

Karato, S. (2015). Some notes on hydrogen-related point defects and their role in the isotope exchange and electrical conductivity in olivine. *Physics of the Earth and Planetary Interiors*, *248*, 94–98. https://doi.org/10.1016/j.pepi.2015.08.007

Katsura, T., Yoneda, A., Yamazaki, D., Yoshino, T., & Ito, E. (2010). Adiabatic temperature profile in the mantle. *Physics of the Earth and Planetary Interiors*, *183*(1-2), 212–218. https://doi.org/10.1016/j.pepi.2010.07.001

Keppler, H., & Smyth, J. R. (2006). Water in nominally anhydrous minerals. *Reviews in Mineralogy and Geochemistry*, *62*, 1–478. https://doi.org/10.1007/978-94-011-4465-0_22

Kohlstdt, D. L., & Mackwell, S. J. (1998). Diffusion of hydrogen and intrinsic point defects in olivine. *Zeitschrift für Physikalische Chemie*, *207*(Part_1_2), 147–162. https://doi.org/10.1524/zpch.1998.207.Part_1_2.147

Kuvshinov, A., & Olsen, N. (2006). A global model of mantle conductivity derived from 5 years of CHAMP, Ørsted, and SAC-C magnetic data. *Geophysical Research Letters*, *33*, L18301. https://doi.org/10.1029/2006GL027083

Lizarrlde, D., Chave, A. D., Hirth, G., & Schultz, A. (1995). A Northern Pacific mantle conductivity profile from long-period magnetotelluric sounding using Hawaii-to-California submarine cable data. *Journal of Geophysical Research*, *100*(B9), 17,837–17,854. https://doi.org/10.1029/95JB01244

Naif, S., Key, K., Constable, S., Evans, R. L., & L, R. (2013). Melt-rich channel observed at the lithosphere-asthenosphere boundary. *Nature*, *495*(7441), 356–359. https://doi.org/10.1038/nature11939

Neal, S. L., Mackie, R. L., Larsen, J. C., & Schultz, A. (2000). Variations in the electrical conductivity of the upper mantle beneath North America and the Pacific Ocean. *Journal of Geophysical Research*, *105*(B4), 8229–8242. https://doi.org/10.1029/1999JB900447

Novella, D., Jacobsen, B., Weber, P. K., Tyburczy, J. A., Ryerson, F. J., & Du Frane, W. L. (2017). Hydrogen self-diffusion in single crystal olivine and electrical conductivity of the Earth's mantle. *Scientific Reports*, *7*(1), 5344. https://doi.org/10.1038/s41598-017-05113-6

Paterson, M. S. (1982). The determination of hydroxyl by infrared absorption in quartz, silicate glasses, and similar materials. *Bulletin de Mineralogie*, *105*, 20–29.

Poe, B. T., Romano, C., Nestola, F., & Smyth, J. R. (2010). Electrical conductivity anisotropy of dry and hydrous olivine at 8 GPa. *Physics of the Earth and Planetary Interiors*, *181*(3-4), 103–111. https://doi.org/10.1016/j.pepi.2010.05.003

Purevjav, N., Okuchi, T., Tomioka, N., Abe, J., & Harjo, S. (2014). Hydrogen site analysis of hydrous ringwoodite in mantle transition zone by pulsed neutron diffraction. *Geophysical Research Letters*, *41*, 6718–6724. https://doi.org/10.1002/2014GL061448

Rudnick, R. L., McDonough, W. F., & O'Connell, R. J. (1998). Thermal structure, thickness and composition of continental lithosphere. *Chemical Geology*, *145*(3-4), 395–411. https://doi.org/10.1016/s0009-2541(97)00151-4

Sano-Furukawa, A., Kuribayashi, T., Komatsu, K., Yagi, T., & Ohtani, E. (2011). Investigation of hydrogen sites of wadsleyite: A neutron diffraction study. *Physics of the Earth and Planetary Interiors*, *189*(1-2), 56–62. https://doi.org/10.1016/j.pepi.2011.07.003

Sarafian, E., Evans, R. L., Collins, J. A., Elsenbeck, J., Gaetani, G. A., Gaherty, J. B., et al. (2015). The electrical structure of the central Pacific upper mantle constrained by the NoMelt experiment. *Geochemistry, Geophysics, Geosystems*, *16*, 1115–1132. https://doi.org/10.1002/2014GC005709

Schultz, A., Kurtz, R. D., Chave, A. D., & Jones, A. G. (1993). Conductivity discontinuities in the upper mantle beneath a stable craton. *Geophysical Research Letters*, *20*(24), 2941–2944. https://doi.org/10.1029/93GL02833

Shatskiy, A., Litasov, K. D., Matsuzaki, T., Shinoda, K., Yamazaki, D., Yoneda, A., et al. (2009). Single crystal growth of wadsleyite. *American Mineralogist*, *94*(8-9), 1130–1136. https://doi.org/10.2138/am.2009.3150

Sun, W., Yoshino, T., Sakamoto, N., & Yurimoto, H. (2015). Hydrogen self-diffusivity in single crystal ringwoodite: Implications for water content and distribution in the mantle transition zone. *Geophysical Research Letters*, *42*, 6582–6589. https://doi.org/10.1002/2015GL064486

Sun, W., Yoshino, T., Sakamoto, N., & Yurimoto, H. (2018). Supercritical fluid in the mantle transition zone deduced from H–D interdiffusion of wadsleyite. *Earth and Planetary Science Letters*, *484*, 309–317. https://doi.org/10.1016/j.epsl.2017.12.032

Tarits, P., Hautot, S., & Perrier, F. (2004). Water in the mantle: Results from electrical conductivity beneath the French Alps. *Geophysical Research Letters*, *31*, L06612. https://doi.org/10.1029/2003GL019277

Turcotte, D. L., & Schubert, G. (1982). *Geodynamics* (Vol. 450). New York: John Wiley & Sons, Inc.

Wang, D., Mookherjee, M., Xu, Y., & Karato, S. (2006). The effect of water on the electrical conductivity of olivine. *Nature*, *443*(7114), 977–980. https://doi.org/10.1038/nature05256

Xue, X., Kanzaki, M., Turner, D., & Loroch, D. (2017). Hydrogen incorporation mechanisms in forsterite: New insights from ^{1}H and ^{29}Si NMR spectroscopy and first-principles calculation. *American Mineralogist*, *102*(3), 519–536. https://doi.org/10.2138/am-2017-5878

Yang, X. (2012). Orientation-related electrical conductivity of hydrous olivine, clinopyroxene and plagioclase and implications for the structure of the lower continental crust and uppermost mantle. *Earth and Planetary Science Letters*, *317-318*, 241–250. https://doi.org/10.1016/j.epsl.2011.11.011

Yoshino, T., & Katsura, T. (2013). Electrical conductivity of mantle minerals: Role of water in conductivity anomalies. *Annual Review of Earth and Planetary Sciences*, *41*, 605–628. https://doi.org/10.1146/annurev-earth-050212-124022

Yoshino, T., Manthilake, G., Matsuzaki, T., & Katsura, T. (2008). Dry mantle transition zone inferred from the conductivity of wadsleyite and ringwoodite. *Nature*, *451*, 326–329. https://doi.org/10.1038/nature06427

Yoshino, T., Matsuzaki, T., Shatskiy, A., & Katsura, T. (2009). The effect of water on the electrical conductivity of olivine aggregates and its implications for the electrical structure of the upper mantle. *Earth and Planetary Science Letters*, *288*(1-2), 291–300. https://doi.org/10.1016/j.epsl.2009.09.032

Yoshino, T., Matsuzaki, T., Yamashita, S., & Katsura, T. (2006). Hydrous olivine unable to account for conductivity anomaly at the top of the asthenosphere. *Nature*, *443*(7114), 973–976. https://doi.org/10.1038/nature05223

Zhang, B., Yoshino, T., Yamazaki, D., Manthilake, G., & Katsura, T. (2014). Electrical conductivity anisotropy in partially molten peridotite under shear deformation. *Earth and Planetary Science Letters*, *405*, 98–109. https://doi.org/10.1016/j.epsl.2014.08.018